Adaptive Model Predictive Control-Based Power Management for Fuel Cell–Battery–Supercapacitor Systems in More-Electrified Aircraft

Morad Yazdani, Navid Vafamand, Siavash Yari, Akhtar Hussain, Innocent Kamwa
Department of Electrical and Computer Engineering
Université Laval
Québec, Canada
(morad.yazdani.1, navid.vafamand.1, siavash.yari.1)@ulaval.ca , (akhtar.hussain, innocent.kamwa)@gel.ulaval.ca

***Abstract*—This paper proposes a power management strategy for a hybrid energy storage system (HESS) comprising a fuel cell (FC), battery(BT), and super capacitor (SC) for onboard microgrids in more-/all-electric aircrafts. An energy management system (EMS) based on model predictive control (MPC) allocates power between the battery and SC during both charging and discharging. Unlike fixed-cutoff filter schemes, the proposed controller adaptively tunes the filter bandwidth based on current dynamics and battery state of charge (SoC), and applies SoC-driven participation factors to enforce operating limits. The MPC cost function promotes smooth battery power and assigns fast transients to the SC while satisfying SoC and converter constraints via a convex quadratic program solved in real time. The approach is validated in MATLAB/Simulink on a representative FC–BT–SC onboard microgrid, demonstrating fast DC-bus voltage recovery, maintenance of BT/SC SoC within admissible ranges, increased SC utilization, and reduced battery stress compared with fixed-cutoff and purely rule-based baselines. These results suggest that the proposed MPC-based EMS offers a practical approach to enhancing voltage regulation and prolonging battery longevity in aviation microgrids.**

***Index Terms*—Energy management systems, Hybrid energy storage systems, Model predictive control, More-electric aircraft, Onboard microgrids, Power allocation**

I. Introduction

Aviation industry is under increasing pressure to reduce emissions and fuel consumption, which is accelerating the development of more-electric and all-electric aircraft concepts in which hydraulic and pneumatic subsystems are progressively replaced by electrically supplied ones [1], [2]. In these platforms, the electrical power system is implemented as an onboard AC/DC microgrid that delivers power to flight-control actuators, avionics, environmental control systems, and, in some architectures, electric propulsion, under strict constraints on weight, reliability, and power quality [3], [4]. The onboard microgrid must supply rapidly varying and highly pulsed loads while keeping the DC-bus voltage within tight limits and ensuring safe operation of power electronic converters [5], [6].

Since the primary sources are typically sized close to the average power demand and have limited dynamic capability, additional energy storage is required to buffer fast load changes, support peak power, and improve overall efficiency [7]. Hybrid energy storage systems (HESS) that combine high-energy batteries with high-power supercapacitors, and in some architectures also fuel cells, exploit complementary energy- and power-density characteristics and are increasingly investigated for on-board aircraft power systems [8]. In particular, fuel-cell–battery–supercapacitor configurations can provide the energy needed for cruise while delivering the power density required for takeoff, maneuvering, and large transient loads. In addition, they offer additional degrees of freedom for managing component aging and operating constraints [2], [7]. In such systems, control design plays a central role, i.e., the energy-management and power-sharing strategies should extend battery life, meet power-quality requirements, and achieve fast dynamics while enforcing state of charge (SoC) limits to prevent overcharging/deep-discharging. Therefore, an appropriate supervisory architecture and converter-level controls are required.

To realize such supervisory control in practice, various energy-management and power-sharing schemes have been proposed in the literature. In [9], a filter-based control scheme comprising a low-pass filter (LPF) and a rate limiter is presented for a BT/SC HESS. The demanded power is decomposed into low- and high-frequency components: the low-frequency portion sets the battery converter reference, while the SC compensates the high-frequency component. Despite its simplicity, a fixed LPF cutoff ignores state-dependent factors such as BT/SC SoC and permissible battery charge/discharge rates. Simialrly, in [10], a two-stage variable rate-limit control is proposed for a BT–SC hybrid storage system, where the SC handles transients and the controller optimizes battery charge/discharge rates to reduce stress. In [11] a rule-based controller (RBC) is implemented to regulate renewable generation and coordinate the HESS. However, it requires measurement and communication of power flows from generators, loads, and any additional storage units, [12].

Despite their advantages, filter-based methods are constrained by a fixed cutoff frequency [13].Therefore, in [14], an RBC is employed whose operation fundamentally relies on a fixed filter augmented with decision rules. A participation coefficient, scheduled by battery SoC, scales the LPF output

979-8-3315-8138-1

current to allocate power between battery and SC. in [15] proposes a battery/SC HESS with an energy management strategy (EMS) that combines rule-based logic and fuzzy control, where the fuzzy controller adaptively tunes the filter cutoff frequency to optimize power sharing. In [16] , A BT-SC HESS is considered. To overcome the limitations of conventional rule-based and fuzzy EMS, Particle Swarm Optimization (PSO) is used under nominal conditions to optimize the fuzzy membership functions with energy loss as the fitness.

Although filter-based and rule-based strategies are widely used in FC–battery–SC HESS architectures, they suffer from notable limitations. Fixed-cutoff LPF methods lack adaptability to SoC variations, converter constraints, and transient severity, often resulting in suboptimal power sharing and increased battery stress. Rule-based controllers, while simple, rely on heuristic tuning and may fail under fast, unpredictable load changes. Most existing approaches treat charging and discharging asymmetrically and do not jointly account for SoC management, transient power allocation, and converter limits. These limitations motivate the need for a systematic and adaptive control framework for coordinated FC–battery–SC operation.

Motivated by the limitations of existing HESS controllers, we propose a model predictive control (MPC)-based EMS for HESS in more/all-electric aircraft. Compared with prior approaches, the controller allocates power between the battery and SC in charging/discharging modes. The EMS is designed to compensate fuel-cell power shortfalls, protect the battery from fast and oscillatory power components, and regulate the SoC of both storage devices while preserving DC-bus voltage quality.

At each sampling instant, the MPC predicts the evolution of the battery and SC SoC over a finite horizon and selects the corresponding power commands by solving a constrained quadratic optimization problem that enforces power balance, SoC limits, and converter constraints. The cost function penalizes deviations of battery power from a low-pass filtered trend and large changes in battery current. Thus, the optimizer naturally assigns medium-frequency demand components to the battery and high-frequency components to the SC.

II. System Architecture

Fig. 1 shows a representative onboard DC microgrid comprising an FC, a battery pack, an SC, and a time-varying load. The FC interfaces the DC link via a boost converter, whereas the battery and SC connect through bidirectional DC–DC converters for charging and discharging. In operation, the FC supplies the average demand, the battery follows slower variations within its admissible charge–discharge range, and the SC covers short, high-power transients, enabling fast DC-bus voltage recovery, maintaining battery and SC SoC within admissible bounds, increasing SC utilization, and reducing battery stress to improve lifetime.

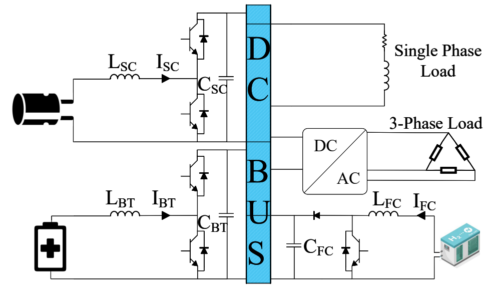

Fig. 1. Configuration of the onboard microgrid.

III. Proposed Energy Management Strategy

Fig. 2 shows the block diagram of the proposed EMS. The FC is sized to operate as the primary energy source during cruise, supplying the DC bus and onboard loads while retaining sufficient margin to charge the battery and SC when surplus power is available. Although the FC provides high energy density, its power density is low; consequently, a BT–SC pair is employed to supply moderate-duration power and fast transients, respectively.

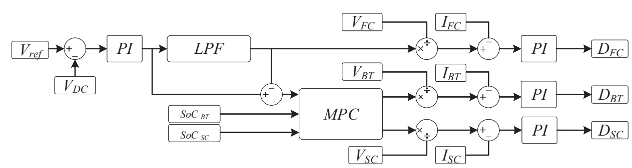

Fig. 2. Block diagram of the control method.

The control system is designed to (i) compensate power shortfalls arising from FC limitations, (ii) shield the battery from oscillatory and high-rate power events, and (iii) maintain and optimally manage the SoC of both battery and SC while meeting DC-bus voltage and power-quality requirements.

A. Model Predictive Controller

The fuel cell cutoff frequency (f_c) sets the primary energy-management bandwidth; (with $f_b \geq f_c$ together with λ_b and R_b sets the battery's effective bandwidth; a small R_{SC} encourages the SC to absorb fast transients.

The proposed control strategy for an onboard aviation microgrid partitions the net power request $P_{\text{tot}}(k)$ into a quasi-DC component allocated to the FC and a complementary, higher-frequency residual allocated to electrochemical storage. The residual demand to be supplied by storage is defined as:

$$P_{res}(k) = P_{tot}(k) - P_{FC}(k) \quad (1)$$

Within each control interval, an MPC determines the battery and SC power commands,$P_b(k)$, $P_{sc}(k)$, such that the instantaneous balance is satisfied while device and state constraints are enforced.

$$P_b(k) + P_{sc}(k) = P_{res}(k) \quad (2)$$

979-8-3315-8138-1

B. Source Modeling

The normalized SoC of the battery and SC are denoted as $SoC_b(k), SoC_{sc}(k) \in [0,1]$, respectively. A linear per-sample SoC model is adopted:

$$SoC_b(k+1) = SoC_b(k) + \alpha_b\, P_b(k), \tag{3}$$

$$SoC_{sc}(k+1) = SoC_{sc}(k) + \alpha_{sc}\, P_{sc}(k), \tag{4}$$

where the power-to-SoC coefficients are computed from usable energies and sampling:

$$a_b = \frac{\sigma_b\, \eta_b\, T_s}{3600\, E_b}, \qquad a_{sc} = \frac{\sigma_{sc}\, \eta_{sc}\, T_s}{3600\, E_{sc}}, \tag{5}$$

With one-step efficiencies $\eta_b, \eta_{sc} \in (0,1]$ and sign parameters $\sigma_b, \sigma_{sc} \in \{+1,-1\}$ chosen to match the power/SoC convention (e.g., $\sigma = -1$ if positive power corresponds to discharge and reduces SoC). Over a prediction horizon of length $N = 4$ and sampling time of 200 sec, the standard lifted model is used:

$$\mathrm{SoC} \;=\; \mathrm{SoC}(k) + S_u\, U \tag{6}$$

$$\mathrm{SoC}(k) = \begin{bmatrix} \mathrm{SoC}_b(k) \\ \mathrm{SoC}_{sc}(k) \end{bmatrix} \tag{7}$$

$$U \;=\; \begin{bmatrix} P_b(0) & P_{sc}(0) & \dots & P_b(N-1) & P_{sc}(N-1) \end{bmatrix}^\top \tag{8}$$

Here, S_{soc} and S_u are the standard prediction matrices obtained from the discrete-time state-space model $x(k+1) = Ax(k) + Bu(k)$ with $A = I_2$ and $B = \mathrm{diag}(a_b, a_{sc})$.

Since the quasi-DC component is supplied by the FC, the residual $P_{\mathrm{res}}(k)$ predominantly contains medium-to-high frequency content. The MPC cost is designed to allocate *intermediate* components to the battery with a smooth profile, and to allocate *high-frequency* components to the SC. A quadratic cost function is formulated as:

$$\begin{aligned} J = \sum_{i=0}^{N-1} \Big(& w_{\mathrm{lp}}\,[P_b(i) - \tilde{P}_b(i)]^2 + \lambda_b\,[P_b(i) - P_b(i-1)]^2 \\ & + R_b\, P_b(i)^2 + R_{SC}\, P_{SC}(i)^2 \Big) \\ & + \sum_{i=1}^{N} \big(w_{\mathrm{SoC},b}\,[\mathrm{SoC}_b(i) - \mathrm{SoC}_b^{\mathrm{ref}}]^2 \\ & \quad + w_{\mathrm{SoC},SC}\,[\mathrm{SoC}_{SC}(i) - \mathrm{SoC}_{SC}^{\mathrm{ref}}]^2 \big) \end{aligned} \tag{9}$$

where $P_b(i-1)$ denotes the previously applied battery command. The slow battery reference $\tilde{P}_b(k)$ is extracted from the residual by a first-order low-pass with cutoff $f_b > f_c$:

$$\tilde{P}_b(k+1) = \alpha_{\mathrm{lp}}\, \tilde{P}_b(k) + (1 - \alpha_{\mathrm{lp}})\, P_{\mathrm{res}}(k), \alpha_{\mathrm{lp}} = e^{-2\pi f_b T_s} \tag{10}$$

In (9), w_{lp} biases the battery toward the slow trend of the residual; λ_b penalizes battery power steps to suppress ripple; and R_b, R_{SC} regularize the per-channel effort.The weights $w_{\mathrm{soc},b}$ and $w_{\mathrm{soc},sc}$ penalize deviations of the battery and SC SoCs from their desired reference values $\mathrm{SOC}_b^{\mathrm{ref}}$ and $\mathrm{SOC}_{sc}^{\mathrm{ref}}$, respectively, so that the optimizer keeps both devices within prescribed operating ranges. In stacked form, the problem is written as the strictly convex quadratic program

$$\min_{U}\; \frac{1}{2}\, U^\top H\, U + f^\top U, \tag{11}$$

Here, $H \succeq 0$ is assembled from the prediction matrices, the effort weights, and the battery forward-difference operator. The vector f collects the linear terms associated with tracking the slow battery reference $\tilde{P}_b(k)$.

IV. Simulation Results

A. Simulation Parameters

To validate the proposed control strategy, the Fig. 1 test system is simulated in MATLAB/Simulink, with parameters summarized in Table I.

TABLE I
System Parameters

Fuel cell Specifications	
Short-circuit current (I_{sc})	8.17 A
Nominal voltage (V_{nom})	24.23 V
Nominal current (I_{nom})	10 A
Nominal power (P_{nom})	242.3 W
Maximum power (P_{max})	400 W
Battery specifications	
Type	Lead–Acid
Ah capacity	12 Ah
Terminal voltage (V_b)	12 V
SC specifications	
Type	Maxwell BM0D0058 E015
Terminal voltage (V_{sc})	15 V
Capacitance	58 F
No. of SC in series	2
DC–DC Converter Parameters	
Circuit Components	$L_{\mathrm{FC}} = 10\,\mathrm{mH},\ C_{\mathrm{FC}} = 440\,\mu\mathrm{F}$ $L_{\mathrm{BT}} = 1.6\,\mathrm{mH},\ C_{\mathrm{BT}} = 440\,\mu\mathrm{F}$ $L_{\mathrm{SC}} = 2\,\mathrm{mH},\ C_{\mathrm{SC}} = 440\,\mu\mathrm{F}$ $C_{\mathrm{dc1}} = 1600\,\mu\mathrm{F},\ C_{\mathrm{dc2}} = 1600\,\mu\mathrm{F}$ $L_s = 5\,\mathrm{mH}$
DC-link voltage (V_{dc})	48 V

B. Power Allocation, and DC-Link Regulation

he DC microgrid is subjected to a time-varying load profile that combines moderate ramps and abrupt step changes in power demand to evaluate how the sources share power.

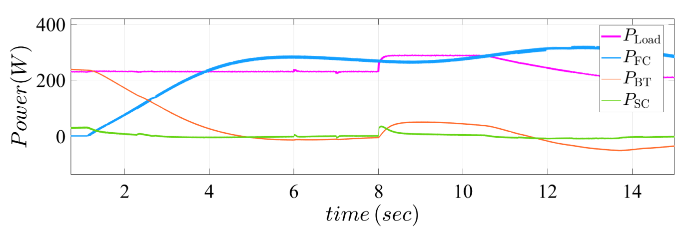

Fig. 3. Power allocation of different sources

Fig. 3 illustrates the power allocation among the FC, battery, and SC during varying load conditions. As the load increases, the FC supplies the majority of the average power, consistent with its role as the primary energy source during cruise. However, due to its limited power density, the FC does not follow rapid variations. Instead, the MPC allocates medium-rate power deviations to the battery, whose electrochemical characteristics allow it to handle moderate transients without

979-8-3315-8138-1

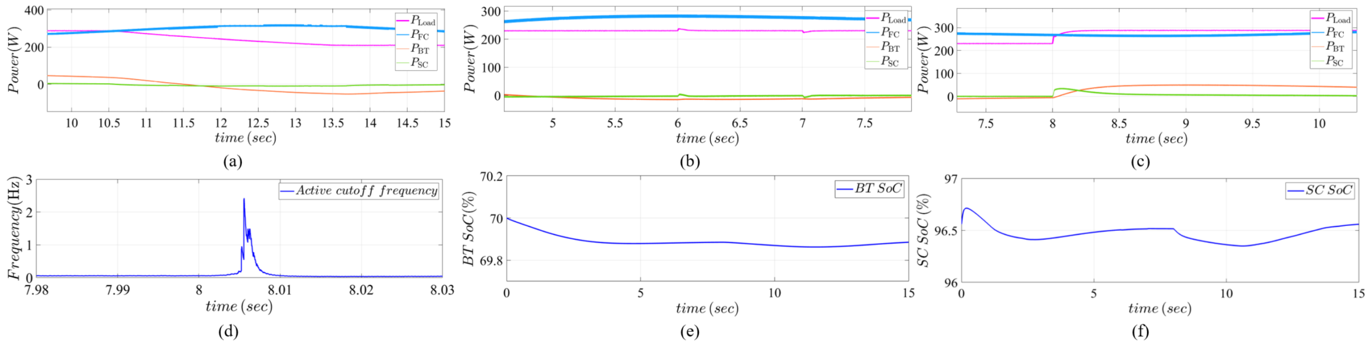

Fig. 4. The Power supplied by different sources during load a) moderate change, b) sudden change, c) sudden massive change. d) Active cutoff frequency (split frequency) e) Battery SoC changes during simulation f) SC SoC changes during simulation

excessive stress. During fast or abrupt load changes, the SC provides the required high-frequency support, momentarily injecting or absorbing power to stabilize the DC link. Once the transient subsides, the SC quickly returns to baseline while the battery and FC resume their steady contributions.

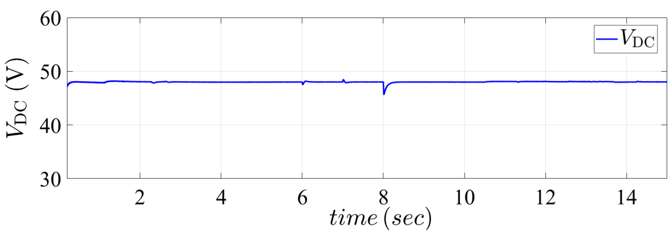

Fig. 5. DC link voltage

Fig. 5 shows the DC-link voltage profile under both moderate and sudden load variations. The voltage quickly settles after initialization and remains tightly regulated around its nominal value throughout the entire simulation. Even during abrupt transients, only minor and short-lived deviations are observed, indicating that the proposed controller effectively coordinates the FC, battery, and SC to maintain DC-link stability.

C. slow to moderate Dynamic Load Transients

During a moderate load variation, Fig. 4(a) illustrates the current trajectories of the FC, battery, and SC. The FC current varies slowly, reflecting its role as the primary energy source that tracks the average power demand. The MPC allocates the dominant portion of the transient power to the battery, whose current exhibits a smooth but noticeable deviation from its initial operating point. In contrast, the SC current remains close to zero, indicating that the supercapacitor is scarcely engaged. This behavior confirms that, for moderate power variations, the battery alone can accommodate the required dynamics without violating its operating limits, while the SC is preserved for faster and more severe transients.

D. Sudden Dynamic Load Transients

Fig. 4(b) shows the current profiles of the FC, battery, and SC during a sudden load change. The SC responds immediately: it current rises sharply to supply the fast-transient power, then quickly settles back to its nominal level. This behavior reflects the SC's role as the high-power, fast-response device in the HESS. In contrast, the battery current remains almost unchanged throughout the event, indicating that the MPC prevents it from experiencing rapid fluctuations that could accelerate degradation. The FC also maintains a nearly constant current due to its slow dynamics.

E. Sudden, High-Magnitude Load Transients

Fig. 4(c) shows the FC, battery, and SC current responses to a sudden large load increase. Immediately, the SC injects a sharp current pulse to absorb the fast transient. The MPC then detects that the demand exceeds the SC's practical limits and reallocates part of the requirement to the battery, so battery current rises to supply the sustained component while SC current decays toward nominal. Owing to the FC's slow dynamics, its current is nearly unchanged initially, but it ramps gradually to assume a larger share of the new steady load.

Fig. 4(d) plots an effective cutoff frequency obtained by fitting the MPC-induced battery response to a demand toP_b low-pass filter, i.e., the controller's effective battery bandwidth. It remains near a low nominal value in steady operation, so the battery tracks mainly low-frequency demand while the SC absorbs ripple. During sharp load changes, a pronounced peak appears, indicating a temporary widening of battery bandwidth to increase its contribution when SC headroom or SoC constraints (or the optimal allocation) limit SC action. After the transient, the frequency returns to baseline, confirming that the MPC automatically restores a slow battery bandwidth under normal operating conditions.

As shown in Fig. 4(e) and Fig. 4(f), the battery and SC SOC profiles reflect their intentionally differentiated dynamic roles. The battery SOC varies slowly, indicating its high-inertia behavior and its role in supplying sustained power, whereas the SC SOC exhibits faster fluctuations, corresponding to its rapid response to transient power demands. This coordinated power-sharing strategy enables smooth and fast power injection and absorption, effectively buffering high-frequency dynamics and reducing battery stress, thereby enhancing overall system reliability and extending battery lifetime.

TABLE II
COMPARISON OF EXISTING CONTROL METHODS WITH THE PROPOSED METHOD

Work	Control method	No. of con-trolled storage	Main advantages	Limitations relative to proposed MPC-based method
[10]	Two-stage control	2	Simple structure; explicit battery range-rate protection	Predefined rate limits; no predictive optimization; SC operation not directly constrained
[11]	RBC EMS with heuristically tuned thresholds	2	Simple computation; straightforward implementation	Heuristic parameter tuning; no explicit optimization; limited adaptability to varying driving cycles
[12]	Decentralized droop-based EMS	2	Low computational complexity; plug-and-play capability	Lacks optimal power allocation; does not explicitly account for component aging or constraints
[13]	Fuzzy-based HESS control	2	Robust parameter variations; intuitive rule design	Rule base grows rapidly with system complexity; no guarantee of optimality
[14]	Filter-based power sharing	2	Effective power split between slow and fast dynamics	Frequency-domain tuning; no predictive capability; limited constraint handling for battery and SC
[15]	Hybrid fuzzy–rule-based EMS	2	Adaptive control tuning; improved robustness to modeling errors	Tuning and design still heuristic; no explicit multi-step prediction; limited handling of hard constraints
[16]	Optimization-based fuzzy control	3	Better compromise between performance and lifetime	Higher design complexity; limited receding-horizon optimization; less systematic constraint treatment than MPC
This paper	Adaptive MPC-based EMS	3	Predictive optimization; fast response; systematic constraint handling; improved battery lifetime and SC utilization	–

As summarized in Table II, existing control strategies rely largely on heuristic or rule-based designs with limited predictive and constraint-handling capabilities, whereas the proposed MPC-based EMS offers systematic optimization and improved energy storage utilization.

V. Conclusion

This paper presented an MPC-based controller for an FC–BT–SC HESS in an onboard DC microgrid. Power is allocated among the FC, battery, and SC by (i) adaptively tuning the filter cutoff frequency based on load/current dynamics and battery SoC and (ii) SoC-driven participation factors that enforce BT/SC limits. Simulations show fast DC-bus voltage recovery and admissible battery/SC SoC under moderate, sudden, and large load changes. The SC supplies high-power transients, the battery tracks slower deviations, and the FC provides average power, increasing SC utilization and smoothing battery current. Overall, the HESS meets onboard power-quality needs while operating safely and reducing battery stress.

Future work will include hardware-in-the-loop validation on a real-time platform, robustness to aging and parameter uncertainty, realistic flight-load profiles, and benchmarking a defined aviation application via head-to-head comparisons with established methods under domain-specific standards and performance metrics for rigorous quantitative assessment.

References

[1] P. J. Ansell and K. S. Haran, “Electrified Airplanes: A Path to Zero-Emission Air Travel,” *IEEE Electrification Magazine*, vol. 8, no. 2, pp. 18–26, 6 2020.

[2] A. Barzkar and M. Ghassemi, “Components of Electrical Power Systems in More and All-Electric Aircraft: A Review,” *IEEE Transactions on Transportation Electrification*, vol. 8, no. 4, pp. 4037–4053, 12 2022.

[3] R. Guo, J. Dong, R. E. Wolleswinkel, R. De Vries, and M. G. Niasar, “Electrical Architecture of 90-Seater Electric Aircraft: A Cable Perspective,” *IEEE Transactions on Transportation Electrification*, vol. 11, no. 2, pp. 6854–6865, 2025.

[4] M. Doff-Sotta, M. Cannon, and J. R. Forbes, “Spacecraft energy management using convex optimisation,” *Energy Conversion and Management: X*, vol. 16, p. 100325, 12 2022.

[5] S. Hosseinnataj, M. Yazdani, M. Shekari, M. Jani, and J. Adabi, “Bidirectional DISO DC-DC Converter Based on Lyapunov Control Strategy,” *2023 14th Power Electronics, Drive Systems, and Technologies Conference, PEDSTC 2023*, 2023.

[6] M. Yazdani, I. Kamwa, J. Adabi, H. Ghoreishy, and H. Porkia, “A Three-Dimensional Space Vector Modulation Method for Reducing Circulating Current and Common Mode Voltage in Three-Phase Four-Leg Parallel Converters,” *2025 IEEE Power & Energy Society General Meeting (PESGM)*, pp. 1–5, 7 2025.

[7] S. Li, P. Zhao, C. Gu, S. Bu, X. Pei, X. Zeng, J. Li, and S. Cheng, “Hybrid Power System Topology and Energy Management Scheme Design for Hydrogen-Powered Aircraft,” *IEEE Transactions on Smart Grid*, vol. 15, no. 2, pp. 1201–1212, 3 2024.

[8] J. Chen, Q. Song, S. Yin, and J. Chen, “On the Decentralized Energy Management Strategy for the All-Electric APU of Future More Electric Aircraft Composed of Multiple Fuel Cells and Supercapacitors,” *IEEE Transactions on Industrial Electronics*, vol. 67, no. 8, pp. 6183–6194, 8 2020.

[9] H. Shayeghi, F. Monfaredi, A. Dejamkhooy, M. Shafie-khah, and J. P. Catalão, “Assessing hybrid supercapacitor-battery energy storage for active power management in a wind-diesel system,” *International Journal of Electrical Power & Energy Systems*, vol. 125, p. 106391, 2 2021.

[10] S. K. Kollimalla, A. Ukil, H. B. Gooi, U. Manandhar, and N. R. Tummuru, “Optimization of Charge/Discharge Rates of a Battery Using a Two-Stage Rate-Limit Control,” *IEEE Transactions on Sustainable Energy*, vol. 8, no. 2, pp. 516–529, 4 2017.

[11] Y. Wang, Z. Sun, and Z. Chen, “Development of energy management system based on a rule-based power distribution strategy for hybrid power sources,” *Energy*, vol. 175, pp. 1055–1066, 5 2019.

[12] A. Azizi, S. Peyghami, H. Mokhtari, and F. Blaabjerg, “Autonomous and decentralized load sharing and energy management approach for DC microgrids,” *Electric Power Systems Research*, vol. 177, p. 106009, 12 2019.

[13] E. Farrokhi, P. Safari, and H. Ghoreishy, “A Rule-based Energy Management Strategy with Current Estimation for Controlling Grid Connected Hybrid Energy Storage System,” in *2023 14th Power Electronics, Drive Systems, and Technologies Conference (PEDSTC)*. IEEE, 1 2023, pp. 1–7.

[14] A. Bharatee, P. K. Ray, and A. Ghosh, “A Power Management Scheme for Grid-connected PV Integrated with Hybrid Energy Storage System,” *Journal of Modern Power Systems and Clean Energy*, vol. 10, no. 4, pp. 954–963, 2022.

[15] S. Hosseinnataj, E. Farrokhi, and J. Adabi, “Novel Hybrid Fuzzy/Rule-based Energy Management for Grid connected Hybrid Energy Storage System,” *2024 9th International Conference on Technology and Energy Management, ICTEM 2024*, 2024.

[16] Z. Liu, C. Wang, and H. Mou, “Optimization-based fuzzy control for the energy management strategy of a hybrid energy storage system,” *2024 IEEE Transportation Electrification Conference and Expo, Asia-Pacific, ITEC Asia-Pacific 2024*, pp. 789–793, 2024.

979-8-3315-8138-1